Supporting Information: P-type Cobaltite Oxide Spinel Enables Efficient Electrocatalytic Oxygen Evolution Reaction

David Doppelbauer,[a,b] Abdalaziz Aljabour,[a] Halime Coskun,[a] He Sun,[a,c] Markus Gusenbauer,[a,b] Julia Lumetzberger,[b] Daniel Primetzhofer,[d] Bogdan Faina,[b] Jiri Duchoslav,[e] Matthias Kehrer,[e] David Stifter,[e] Heiko Groiss,[e,f], Verena Ney,[b] Andreas Ney,[b] and Philipp Stadler*[a,c]

Table of Content

[a] *Institute of Physical Chemistry, Johannes Kepler University Linz, Altenbergerstrasse 69, 4040 Linz, Austria; E-mail: philipp.stadler@jku.at*
[b] *Institute of Semiconductor and Solid State Physics, Johannes Kepler University Linz, Altenbergerstrasse 69, 4040 Linz, Austria.*
[c] *Linz Institute of Technology, Johannes Kepler University Linz, Altenbergerstrasse 69, 4040 Linz, Austria.*
[d] *Department of Physics and Astronomy, Uppsala University, Box 516, 751 20, Uppsala, Sweden.*
[e] *Center for Surface and Nanoanalytics, Johannes Kepler University Linz, Altenbergerstrasse 69, 4040 Linz, Austria.*
[f] *Christian Doppler Laboratory for Nanoscale Phase Transformations, Center for Surface and Nanoanalytics, Johannes Kepler University Linz, Altenberger Str. 69, 4040 Linz, Austria.*
† Electronic Supplementary Information (ESI) available: [details of any supplementary information available should be included here]. See DOI: 00.0000/00000000.

- Table S2: Electrochemical impedance spectra: summary of parameters (membrane and electrolyte resistance and capacitane) as shown in Figure SS14.
- Table S3: Statistical overview of electrocatalytic $Zn_{1.2}Co_{1.8}O_{3.5}$ anodes relating to Figure SS10.
- Figure SS11: Cyclic voltammetry (CV) and 50 h chronoamperometry on Au/Ti-mesh substrate.
- Figure SS12: Corrosion effect on Ti-mesh (anodic growth of TiO_2).
- Figure SS13: Detailed Tafel-slope analysis of as-measured current versus overpotential η.
- Figure SS14: Electrochemical impedance spectroscopy and corresponding equivalent circuit to derive the cell parameters (electrolyte and membrane resistance).
- Figure SS15: Linear sweep voltammograms to large current densities.
- Figure SS16: Determination of the electrochemical surface area by linear sweep voltammetry in organic electrolyte (acetonitrile, 0.1 M TBA-PF_6).
- Figure SS17: Schematic of the electrochemical H-cell.
- Figure SS18: Statistical evaluation of different experiments carried out on the electrocatalytic anodes of $Zn_{1.2}Co_{1.8}O_{3.5}$ grown on (left) Ti-mesh and (right) Al:ZnO.
- Figure SS19: after-electrolysis XPS survey of $Zn_{1.2}Co_{1.8}O_{3.5}$ on titanium with a Zn:Co ratio at approx. 0.65.
- Figure SS20: Hall measurement outline/summary parameters of $Zn_{1.2}Co_{1.8}O_{3.5}$ Hall specimen - van der Pauw specimen; sample grown on sapphire (0001)).
- Figure SS21: Proof of Ohmic-contact to the sample specimen prior Hall-characterization.
- Figure SS22: Details of resistivity measurement (at 300K) of $Zn_{1.2}Co_{1.8}O_{3.5}$ Hall specimen using the van-der-Pauw geometry.
- Figure SS23: Corresponding Hall-characterization (at 300K) using AC-Hall methode supported by LakeShore HMS 8400 cryogenic probe station: AC-magentic fields allow to probe Hall-voltages in low-mobility samples such as the defect-controlled $Zn_{1.2}Co_{1.8}O_{3.5}$.
- Figure SS24: Gas-chromatogram (He) of the anode headspace before/after 1h electrolysis.

Additional tables and equations

Table 1 FWHM analysis of p-doped Zn-Co spinels.

substrate	peak spinel (222) / 2θ	FWHM / 2θ	τ^* / nm
sapphire	38.0 deg	0.25 deg	31.8
rutile	38.092 deg	0.25 deg	32
Ti-mesh (native TiO_2)	38.092 deg	0.28 deg	28.6
Al:ZnO (wurtzite)	38.3 deg	0.39 deg	21

*Scherrer analysis.

Table 2 Electrochemical impedance spectra of electrolysis cell.

WE	CE	$R_{ele.}$ / $\Omega\,cm^{-2}$	$R_{me.}$ / $\Omega\,cm^{-2}$	C / $\mu F\,cm^{-2}$
Pt	Pt	1.8	16	27
$Zn_{1.2}Co_{1.8}O_{3.5}$/Ti-mesh*	Ni	2.0	16	21.3

* Including Ti-corrosion effects. ** WE = working electrode, CE = counter electrode, ele. = electrolyte, me. = membrane.

Table 3 Statistical data.

Anode	$\eta^*_{av.}$ / V	$\eta_{av.}$ / V	$\eta_{min.}$ / V	standard deviation / mV
$Zn_{1.2}Co_{1.8}O_{3.5}$/Ti-mesh	0.35	0.363	0.345	± 6
$Zn_{1.2}Co_{1.8}O_{3.5}$/Al:ZnO	0.41	0.425	0.39	± 7

* at $10\,mA\,cm^{-2}$

Appendix: Scherrer analysis

The domain size (τ) is calculated using the Scherrer formula:

$$\tau = \frac{K \cdot \lambda}{\beta \cdot \cos\theta} \tag{1}$$

with the excitation length $\lambda = 0.15406\,nm$ (Cu $K_{\alpha 1}$), the shape factor $K = 0.89$ (spherical), the Bragg angle θ (deg) of the peak and the (radial) peak full width (at half maximum, FWHM, deg, Figure S7).

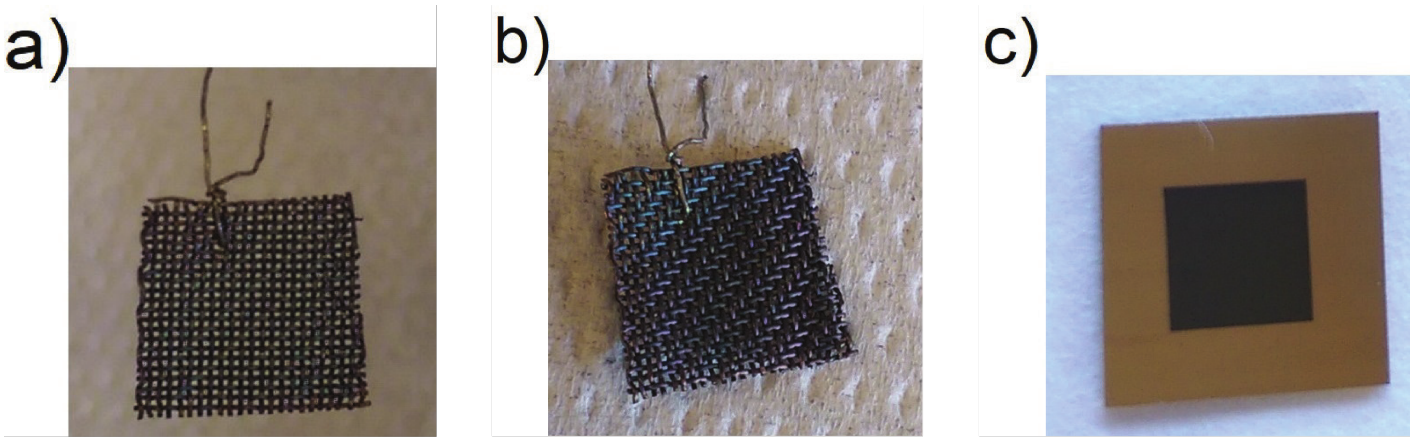

Fig. S1 Samples used for OER characterization: blank Ti-mesh, Ti-mesh covered with $Zn_{1.2}Co_{1.8}O_{3.5}$ and patterned substrate on sapphire (0001) with Al:ZnO as conducting layer buried under $Zn_{1.2}Co_{1.8}O_{3.5}$ and Au, respectively.

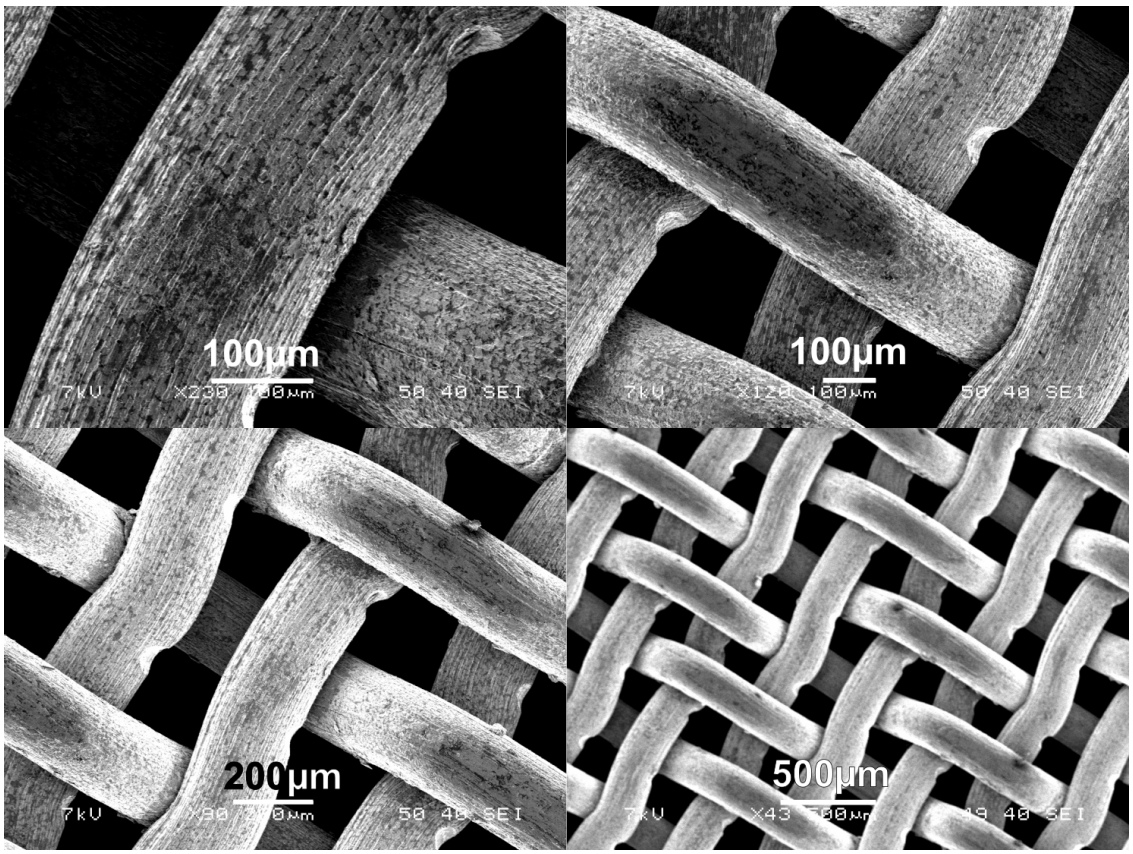

Fig. S2 SEM images of the Ti-mesh: We show the geometric factor of 0.75 (projected versus geometric area).

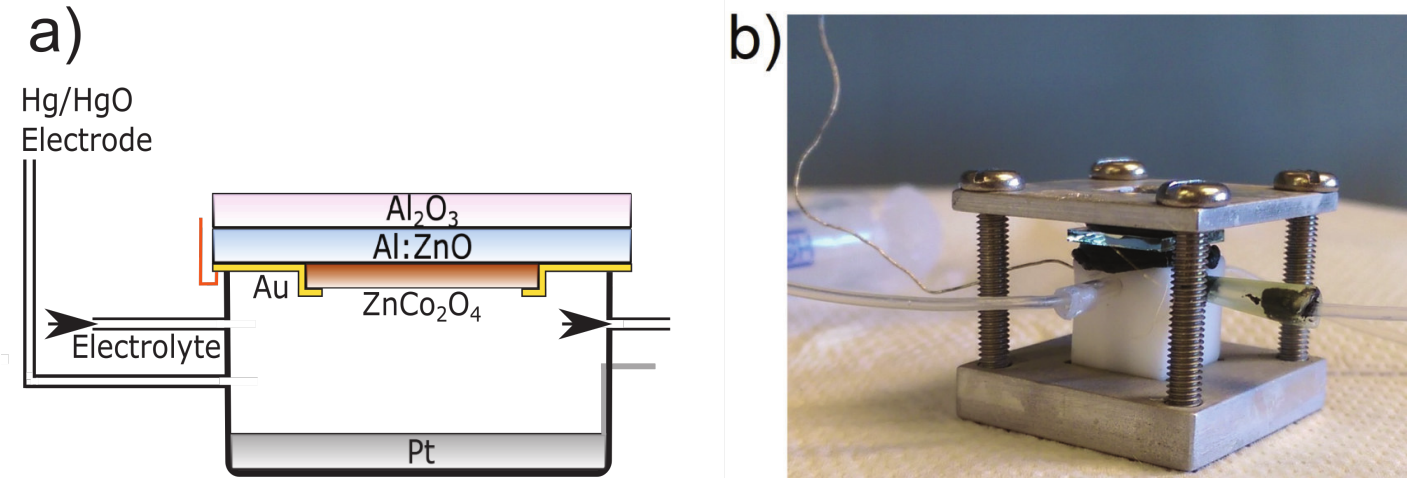

Fig. S3 Al:ZnO as conductive substrate for OER: high-quality Al:ZnO is co-deposited prior the Zn-Co-O spinel on sapphire (0001). To protect the Al:ZnO from dissolution in alkaline media, the conducting oxide is covered in the center with spinel $Zn_{1.2}Co_{1.8}O_{3.5}$ (active area) and, concomitantly, on the edges with Au (schematic in (a)). In (b), the actual electrolysis cell used for characterization is depicted.

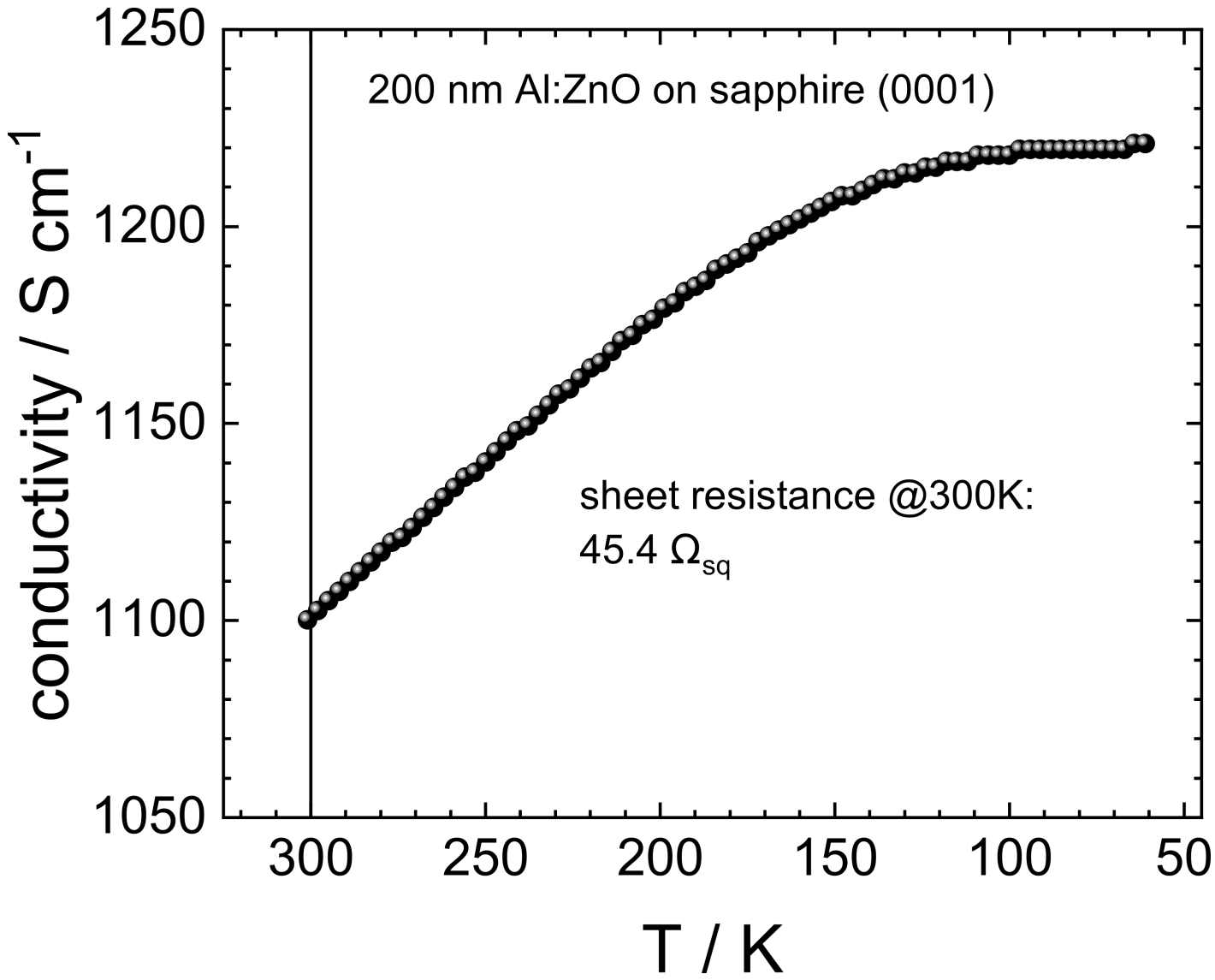

Fig. S4 Conductivity of Al:ZnO on sapphire (0001): Prior the catalytic $Zn_{1.2}Co_{1.8}O_{3.5}$, 200 nm Al:ZnO are deposited (doping at approx. 2% Al) resulting in a conductivity of 1100 S cm^{-1} and a sheet resistance of 45.4 Ω per square.

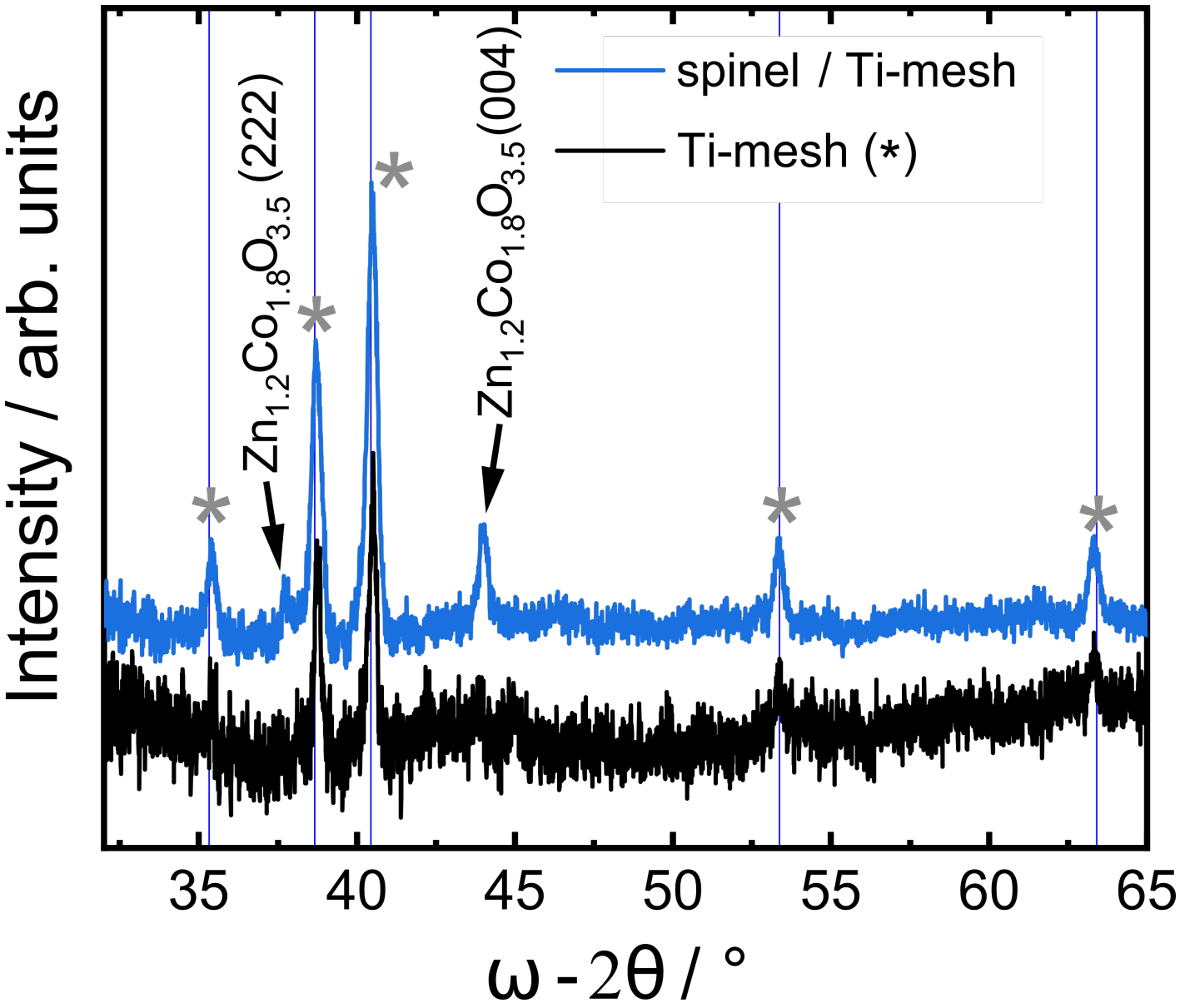

Fig. S5 Ti-mesh calibration: X-ray diffraction patterns of Ti-mesh with and without $Zn_{1.2}Co_{1.8}O_{3.5}$.

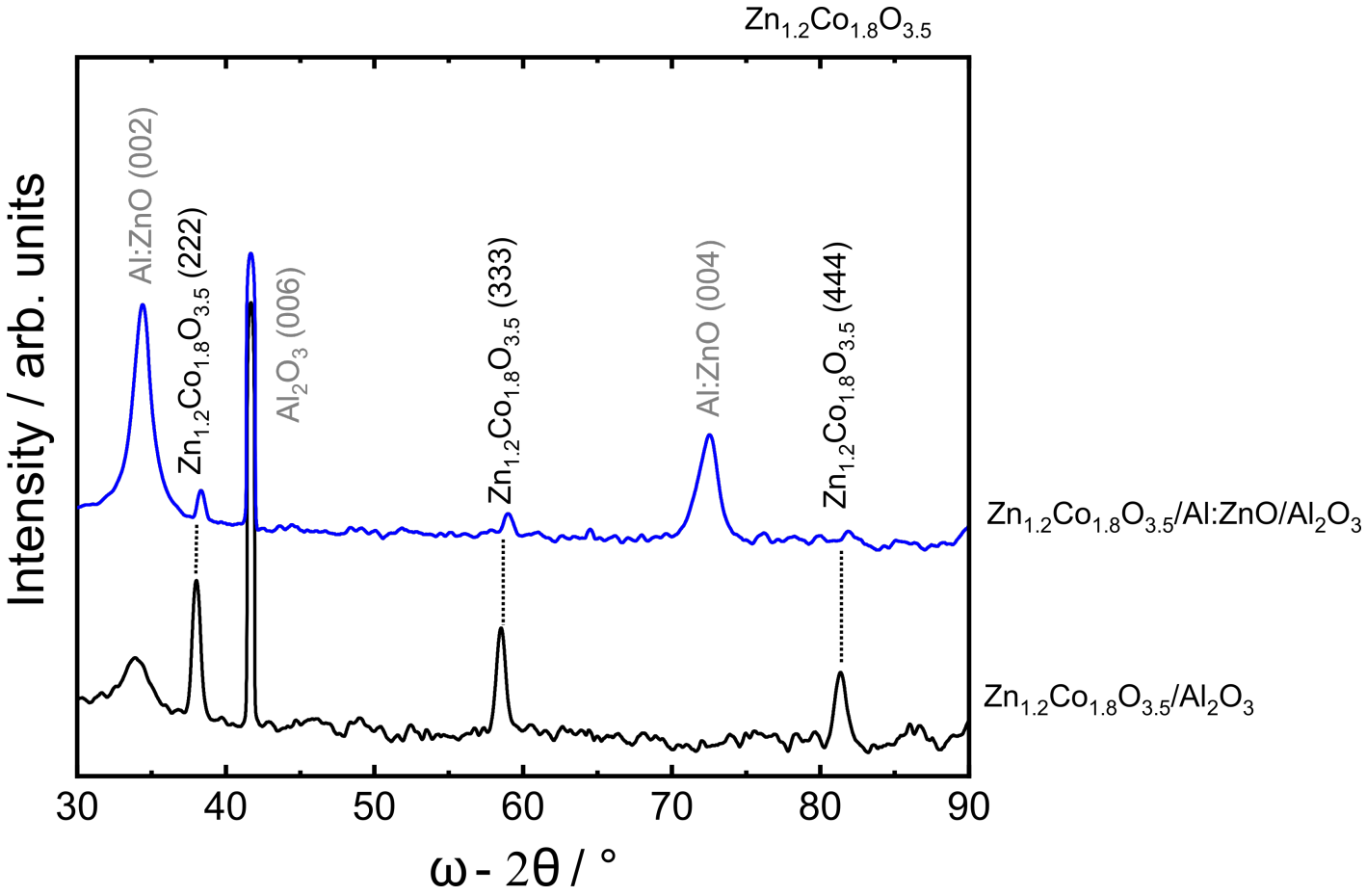

Fig. S6 Detailed diffraction patterns of $Zn_{1.2}Co_{1.8}O_{3.5}$: (222), (333) and (444) pattern on sapphire and Al:ZnO.

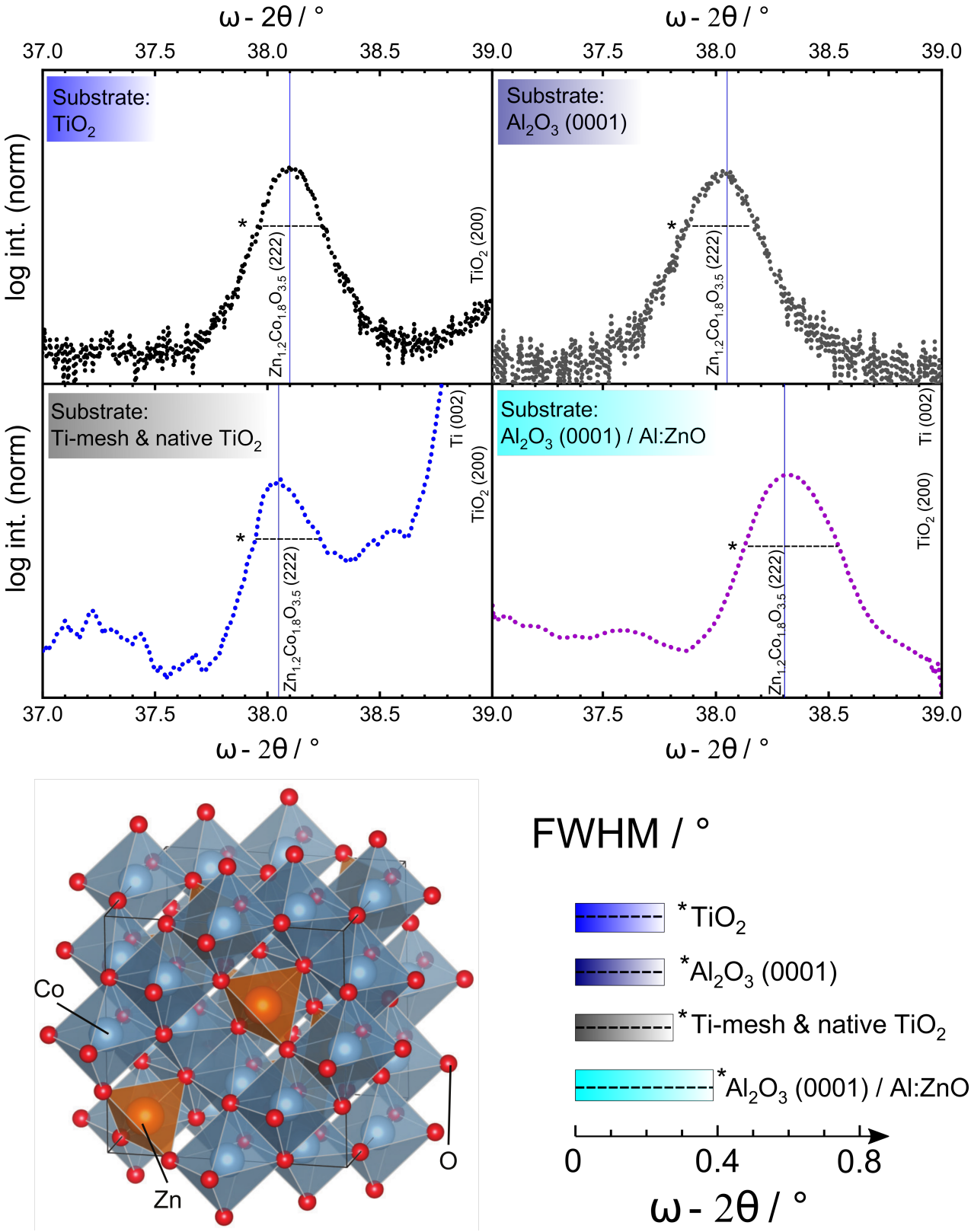

Fig. S7 Comparison of the FWHM/Scherrer analysis: Diffraction peaks of the (222) Zn-Co-O spinel pattern (semi-log scale) on following substrates: TiO_2 (rutile, tetragonal) and Al_2O_3 (sapphire 0001, hexagonal) as the reference substrates; Ti-mesh with native TiO_2 and Al:ZnO (on sapphire 0001, hexagonal) used as electrocatalytic anodes. On the bottom. the spinel we include the structure of the Zn-Co-O system and the corresponding full widths according to the diffraction pattern. From that we calculated the average domain size τ according to equation 1 summarized in Table 1.

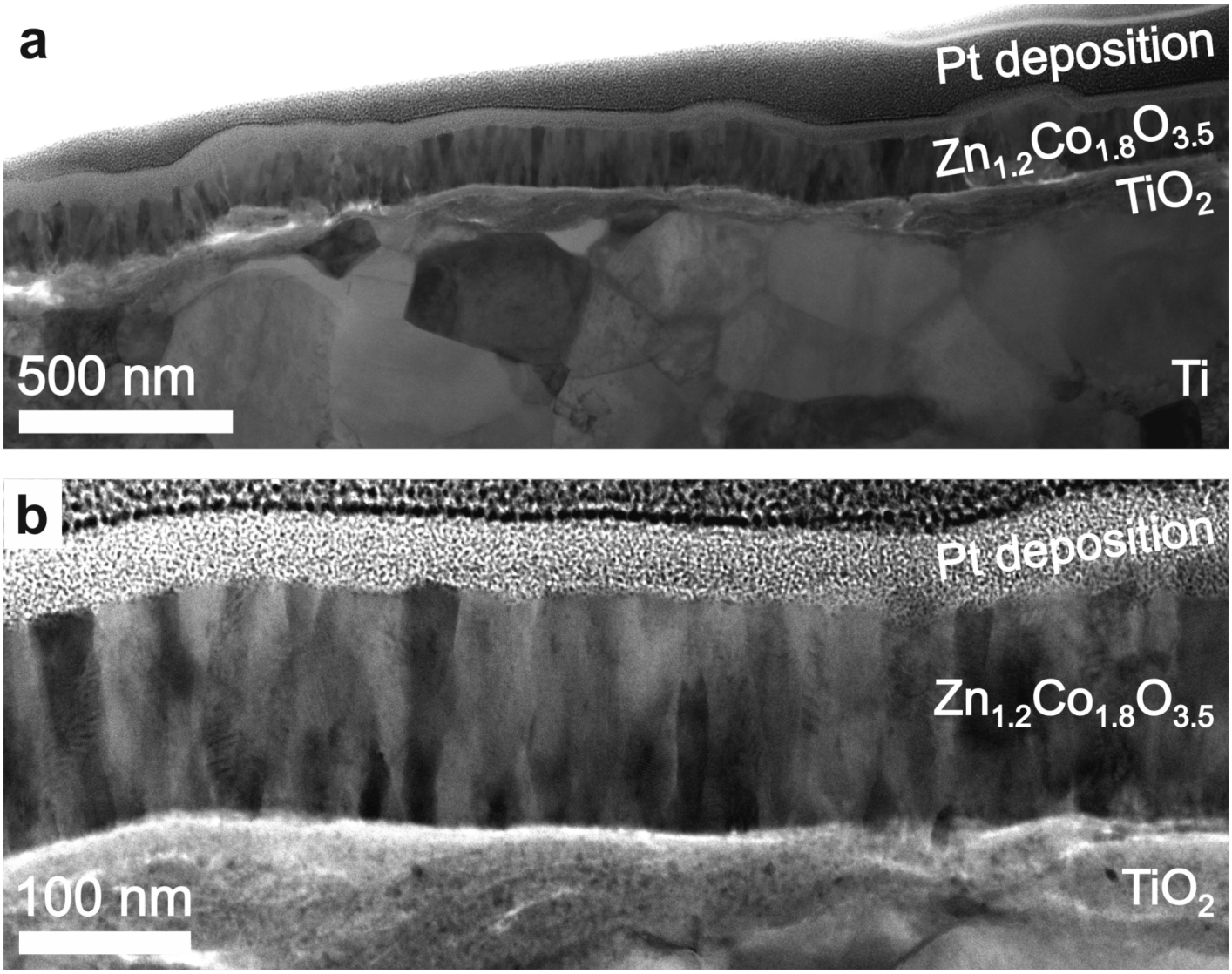

Fig. S8 Structure of the Ti-mesh by bright field STEM: (a) the overview displays the homogeneous thick $Zn_{1.2}Co_{1.8}O_{3.5}$ on top of the TiO_2 covered Ti-mesh. (b) Most of the columnar grains reach from the TiO_2 to the surface with diameters in the region from 10-40 nm.

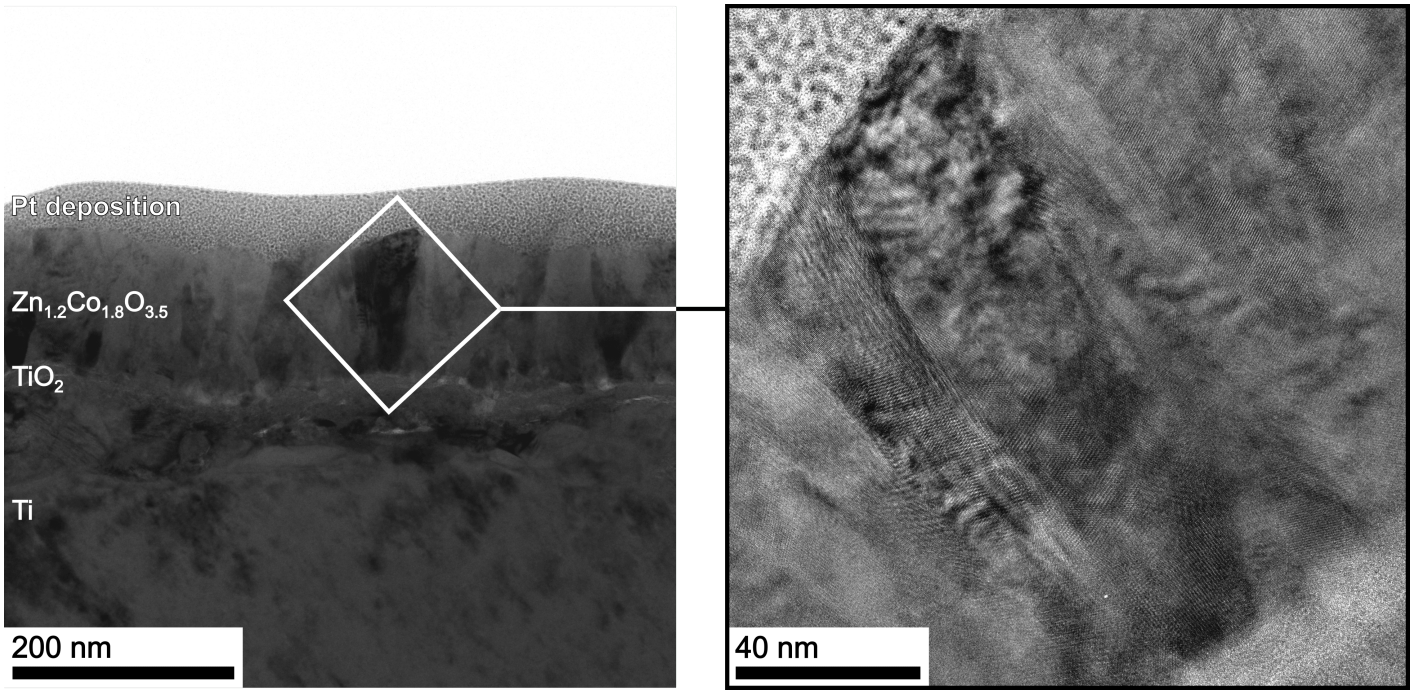

Fig. S9 TEM lattice image of the $Zn_{1.2}Co_{1.8}O_{3.5}$ layer: The lattice fringes of the marked grain and its neighboring grains are well visible in the right-hand high-resolution phase contrast image proving the good crystal quality of the active $Zn_{1.2}Co_{1.8}O_{3.5}$ layer. The average domain size τ corresponds to the XRD Scherrer analysis (Figure S7 and Table S1).

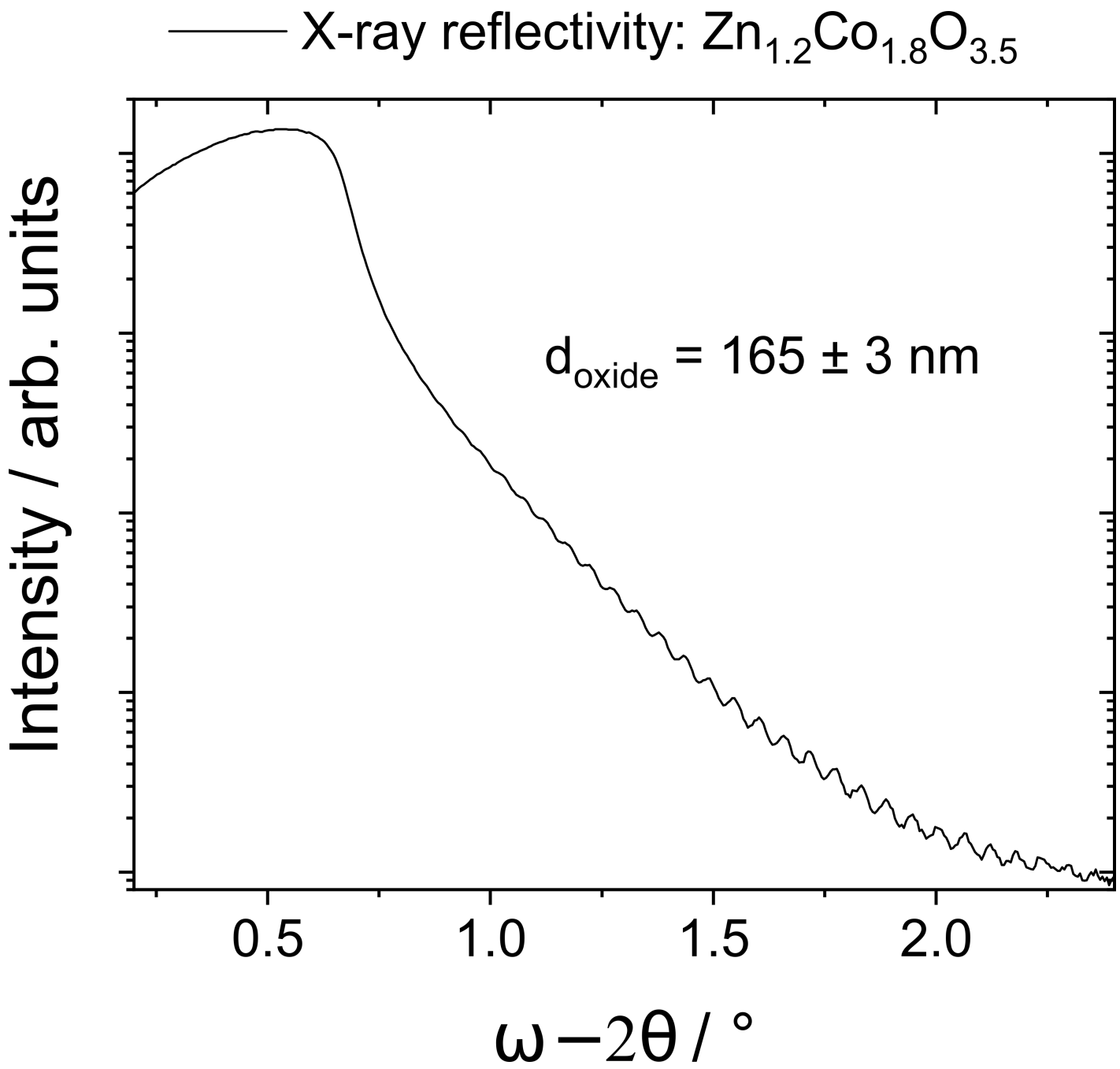

Fig. S10 X-ray reflection measurement on Hall-specimen: $Zn_{1.2}Co_{1.8}O_{3.5}$ grown on sapphire (0001) for the van-der-Pauw Hall specimen yielding 165 ±3 nm.

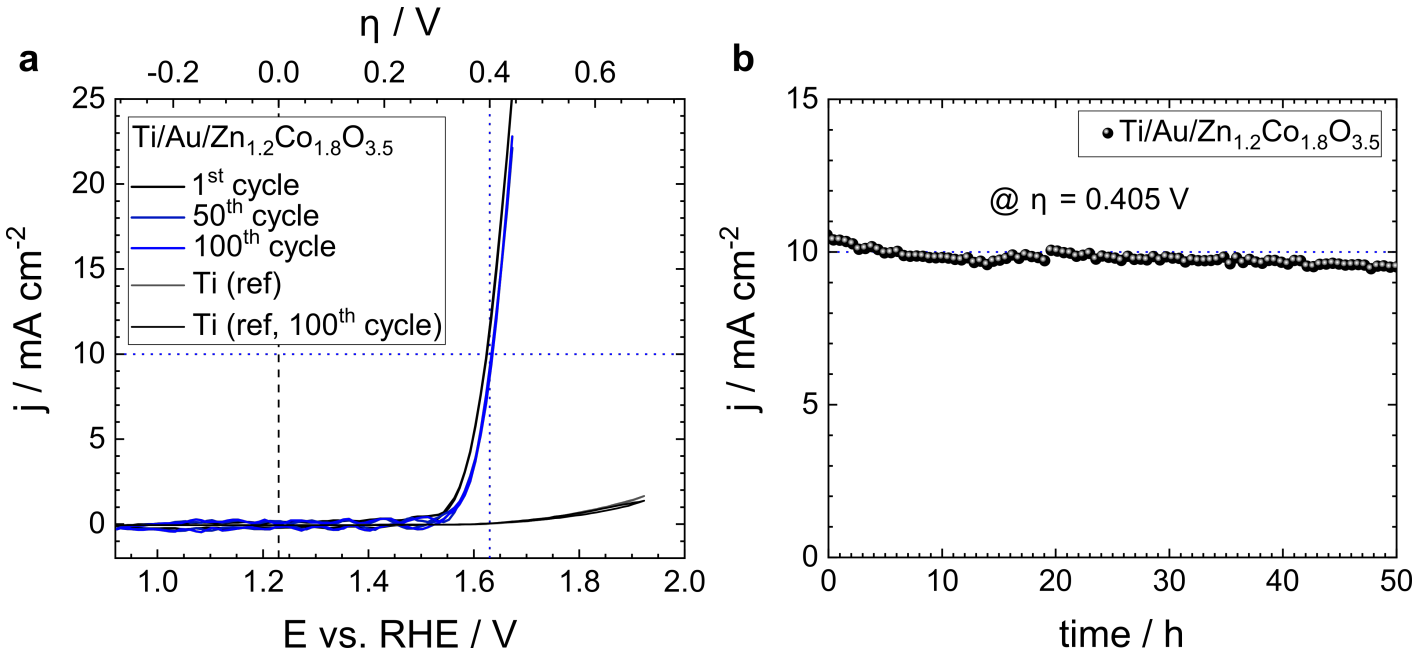

Fig. S11 Electrochemical characterization of Ti/Au (10 nm) / $Zn_{1.2}Co_{1.8}O_{3.5}$. (a) Cyclic voltammetry and (b) chronoamperometry for 50 h to test the stability at 10 mA cm^{-2}.

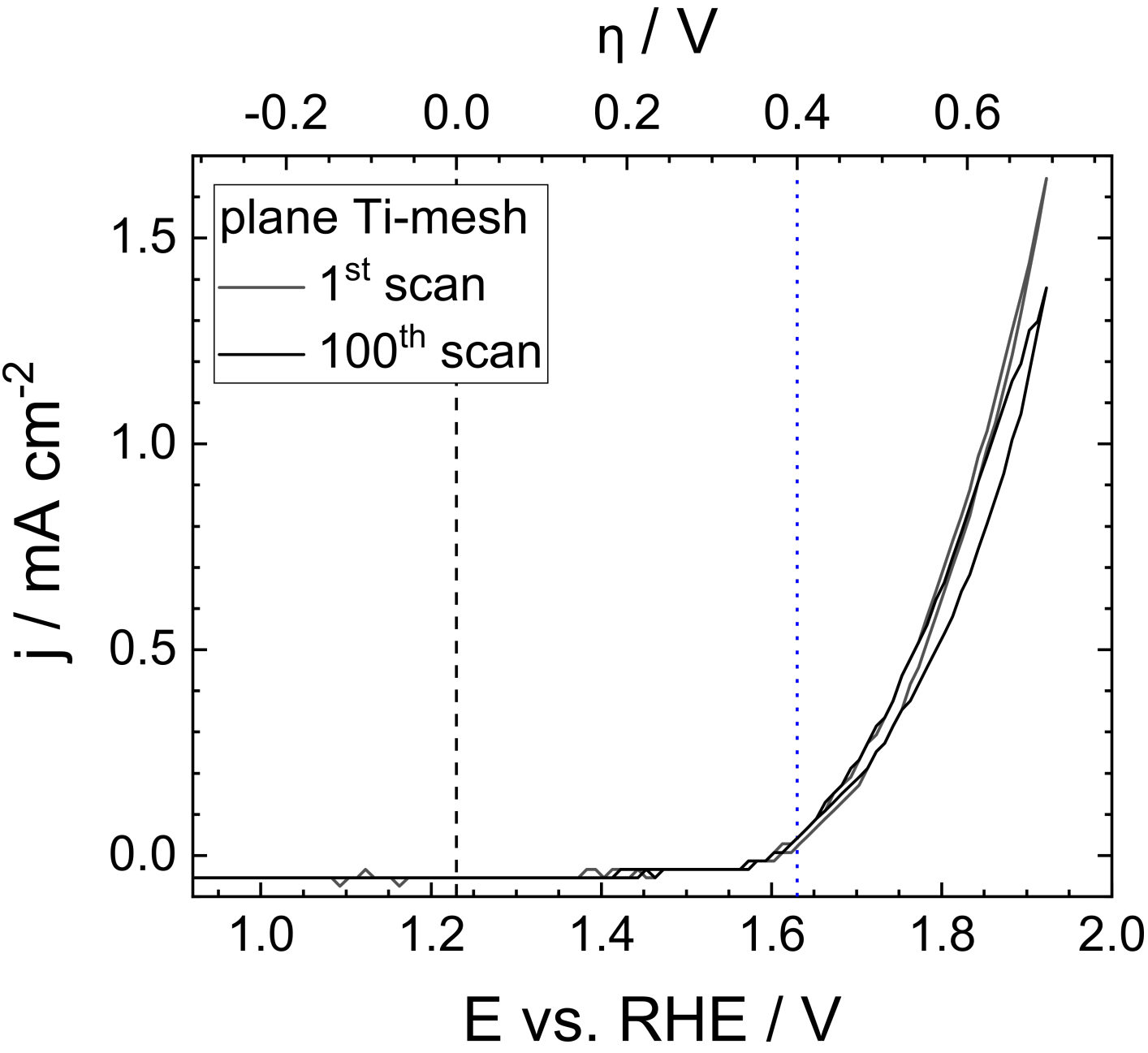

Fig. S12 Ti-corrosion: Cyclic voltammogram reveals an increase of the anodic current after cycling at anodic potentials.

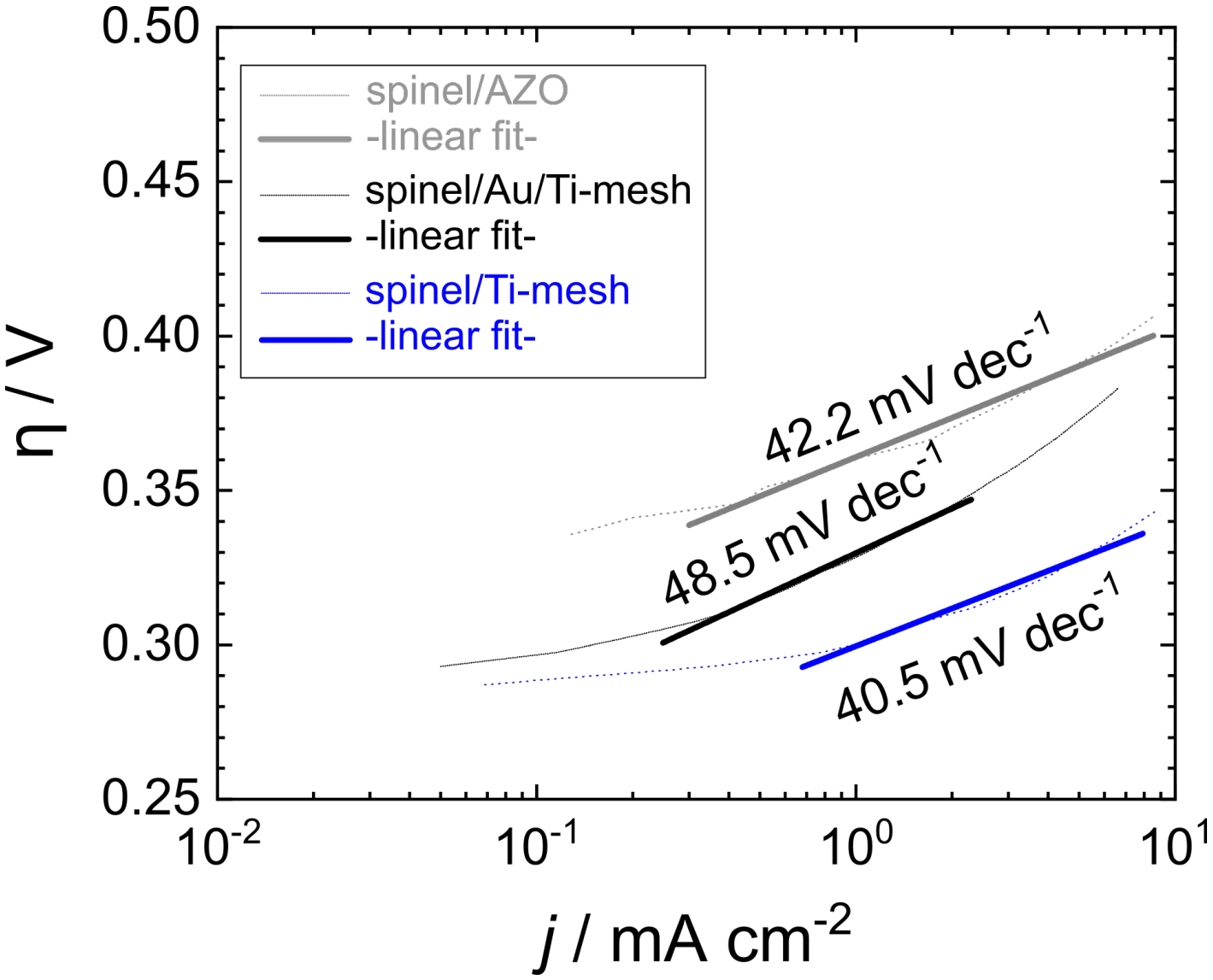

Fig. S13 Detailed Tafel analysis: Extraction of Tafel slopes in the linear regime of the semilogarithmic Tafel-plots.

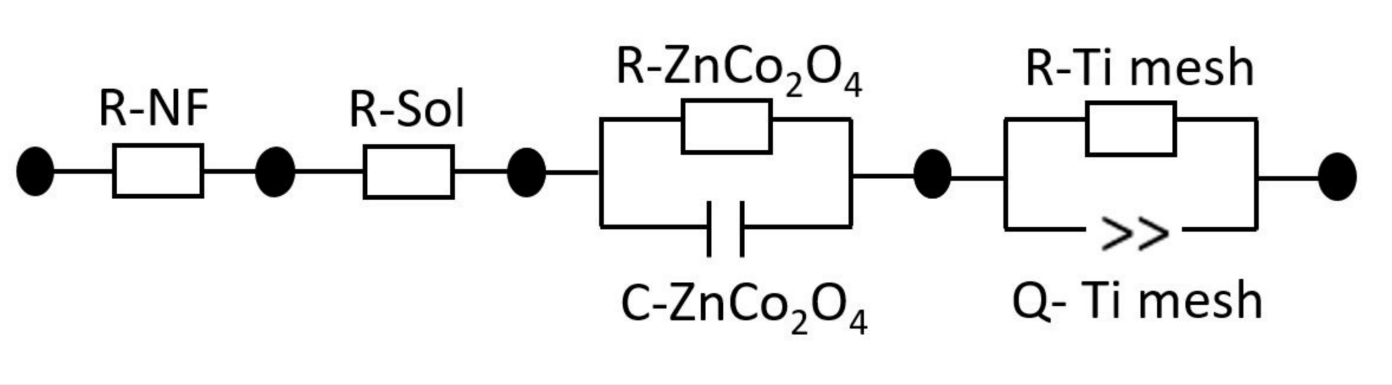

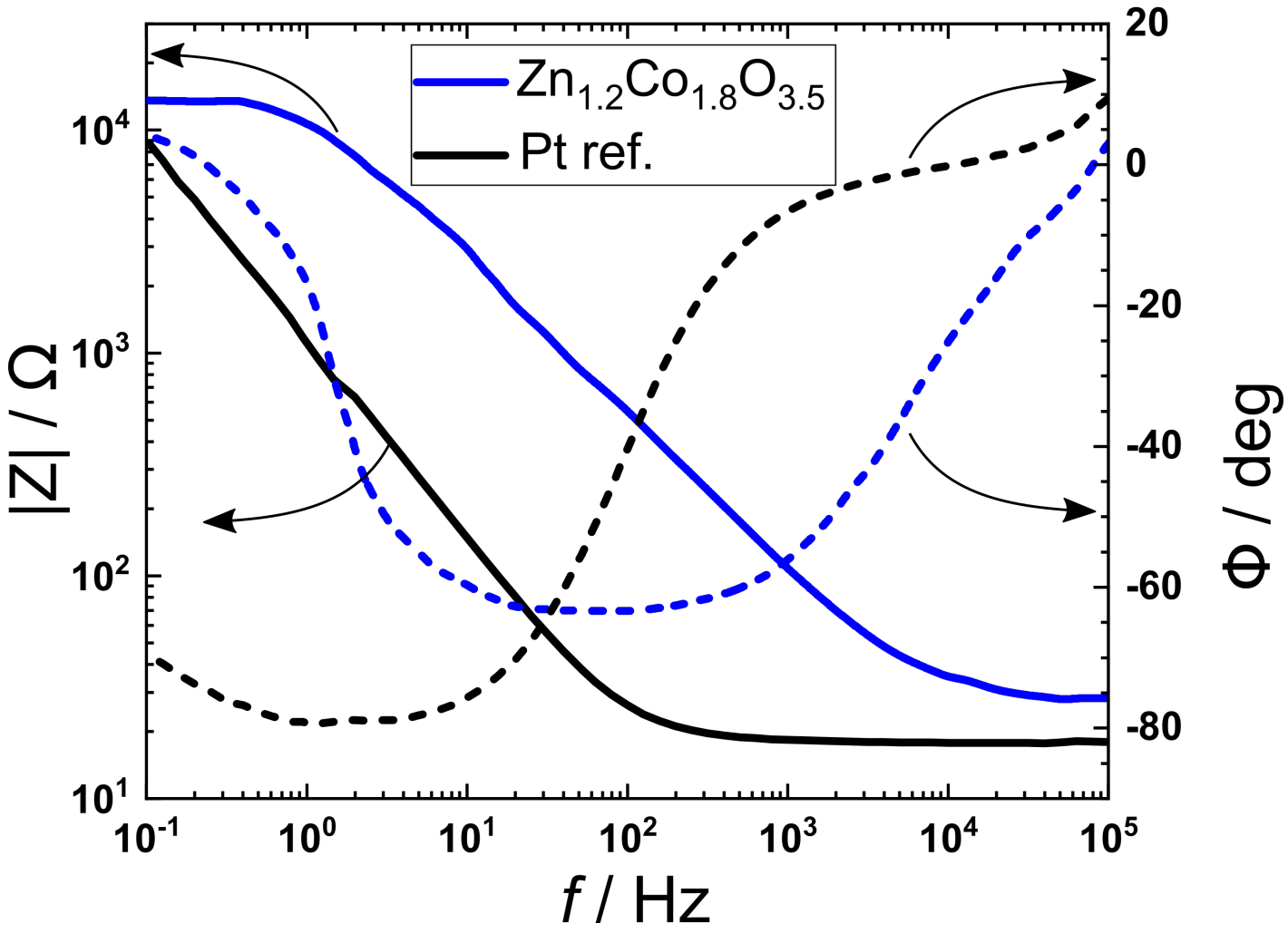

Fig. S14 Electrochemical impedance spectroscopy: The electrochemical cell constants ($R_{electrolyte}$, $R_{membrane}$, capacitance) are presented in Table 2.

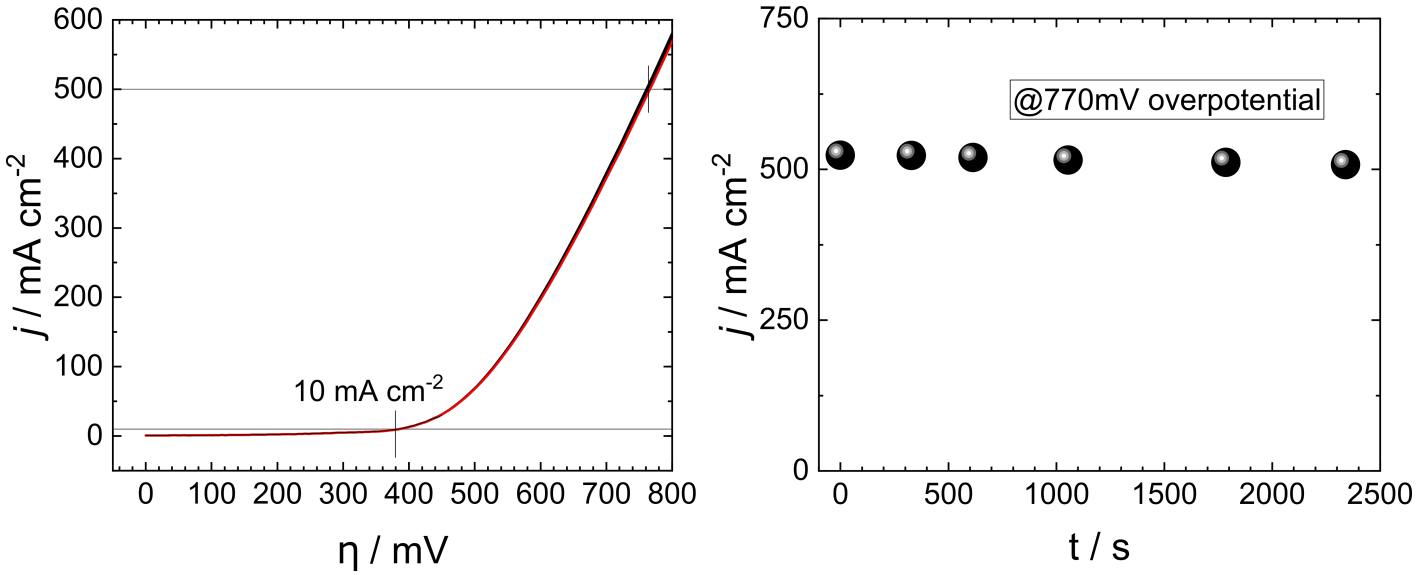

Fig. S15 Linear sweep voltammogram exceeding 500 mA cm^{-2}.

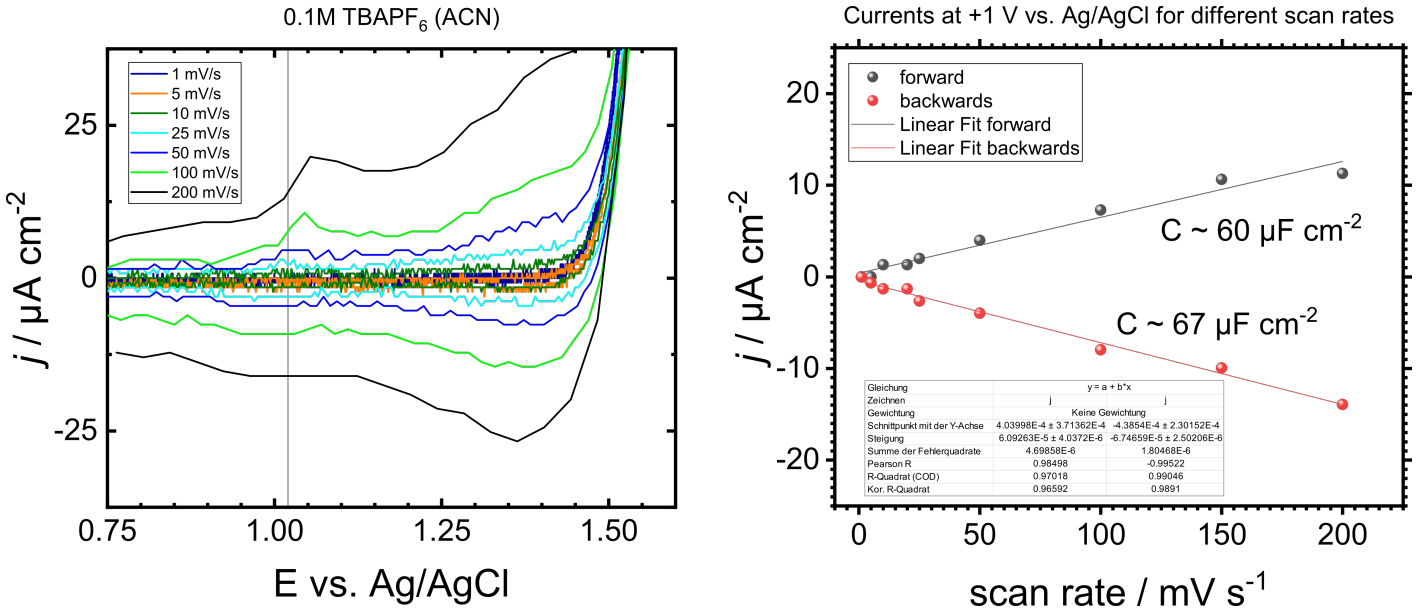

Fig. S16 Current density versus scan rate to determine the electrochemical surface area (ECSA) in organic electrolyte (acetonitrile, 0.1 M TBA-PF_6). The measurement was performed at the equilibrium potential of the O_2 evolution at +1 V vs. Ag/AgCl (quasi) reference elctrode.

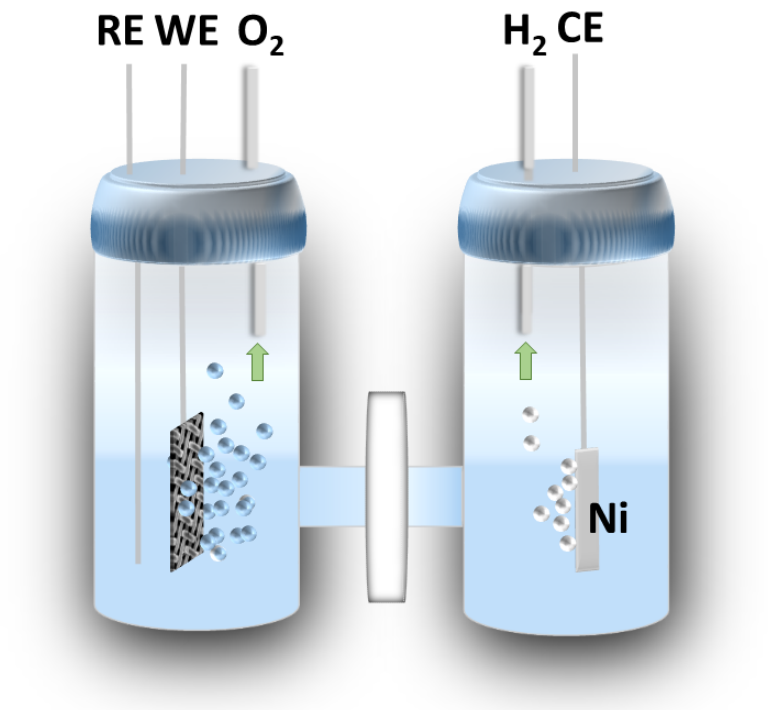

Fig. S17 Schematic of the electrochemical H-cell for conducting the electrocatalytic splitting of water.

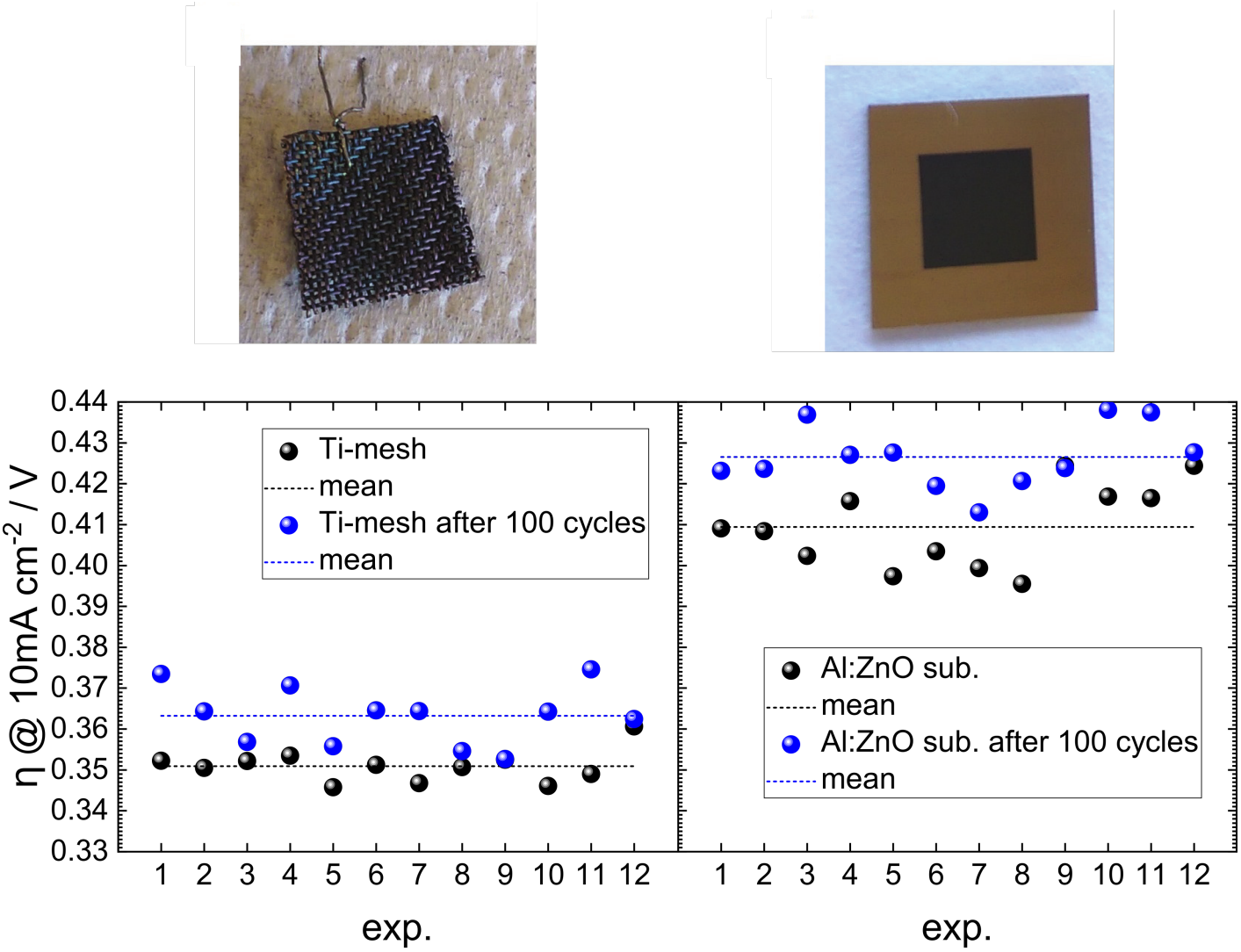

Fig. S18 Statistical evaluation: Different experiments on electrocatalytic anodes: $Zn_{1.2}Co_{1.8}O_{3.5}$ on Ti-mesh and Al:ZnO, respectively.

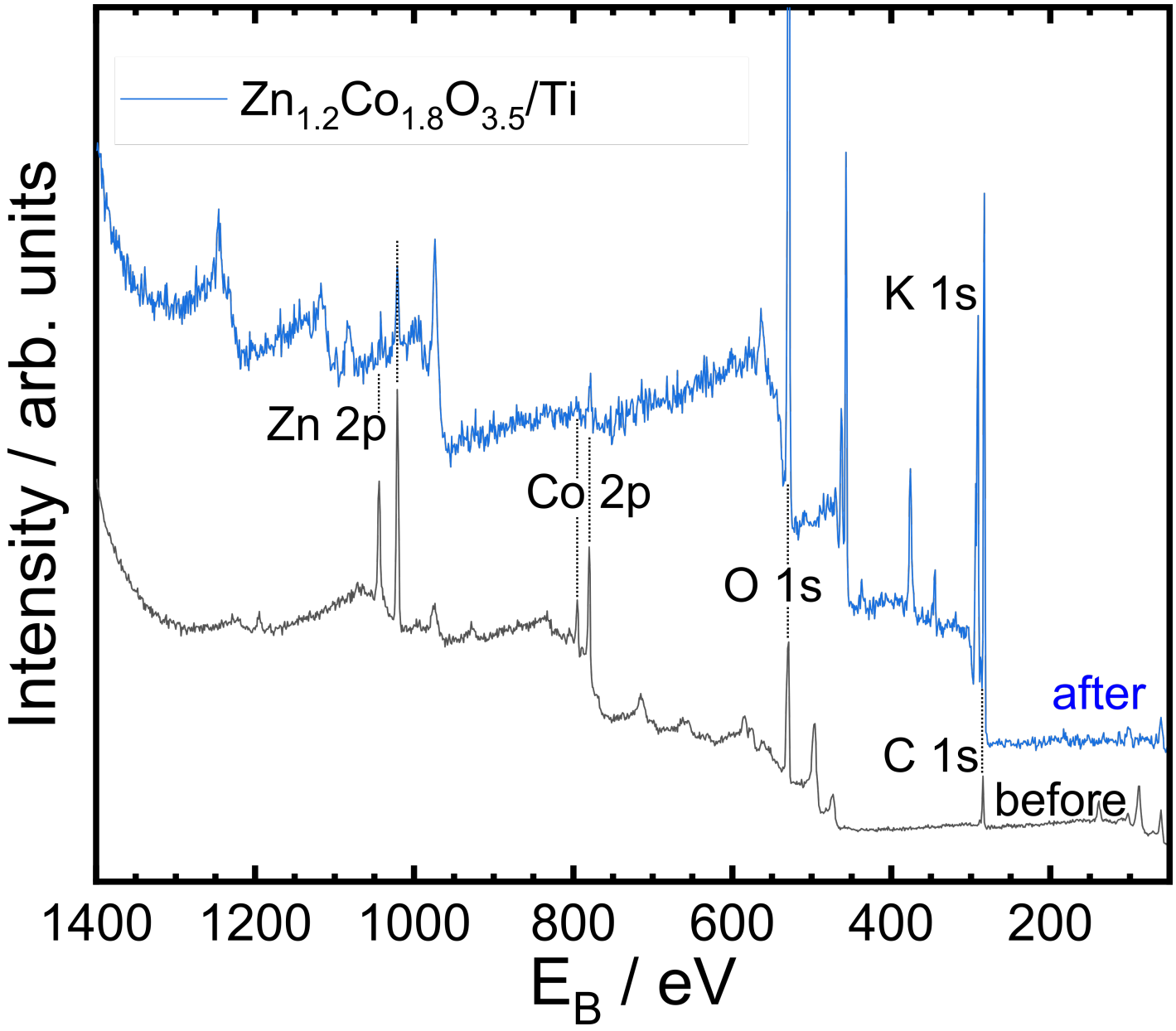

Fig. S19 XPS survey before/after electrolysis of $Zn_{1.2}Co_{1.8}O_{3.5}$ on titanium: surface composition (Zn:Co at ≈ 0.65) remains similar after electrolysis of O_2 for 50 h.

Lake Shore CRYOTRONICS

8400 Series

Step 3.1: Hall measurement (at 300K)

Run-time operator

Sample	
ID:	CoZnOx Spinell
Type:	van der Pauw
Thickness	
t [nm]:	165
Other dimensions	
Lp [mm]:	
Hall factor:	1
Max voltage [V]:	100
Max current [mA]:	20
Gate bias voltage [V]:	0

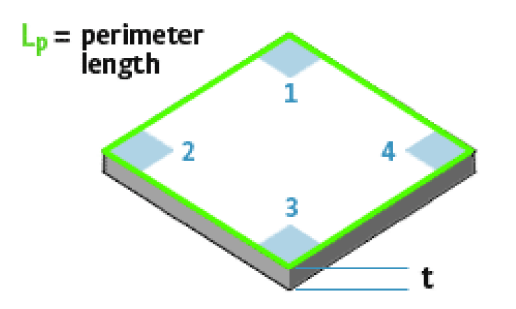

Comment:

Final results			
		Mean value	Limit
μ_H	Hall mobility [cm²/V·s]	4.7167E-2	
	Carrier type	P	
n	Carrier concentration [1/cm³]	1.4382E21	
n_{sheet}	Sheet carrier concentration [1/cm²]	3.0489E16	
R_H	Hall coefficient [cm³/C]	4.3399E-3	
R_{Hsheet}	Sheet Hall coefficient [cm²/C]	2.0471E2	
ρ	Resistivity [Ω·cm]	9.2011E-2	
ρ_{sheet}	Sheet resis+vity [Ω/□]	4.3401E3	
V_H	Hall voltage [V]	1.2800E-6	
	Phase [deg.]	-7.7	
	Worst case Ohmic check correlation (1-3)	9.9893E-1	

Measurement comment

Fig. S20 Summary of Hall measurement: A LakeShore 8400 Hall measurement system was used to measure the van der Pauw-type specimen of $Zn_{1.2}Co_{1.8}O_{3.5}$ grown on sapphire (0001) (here shown at 300K).

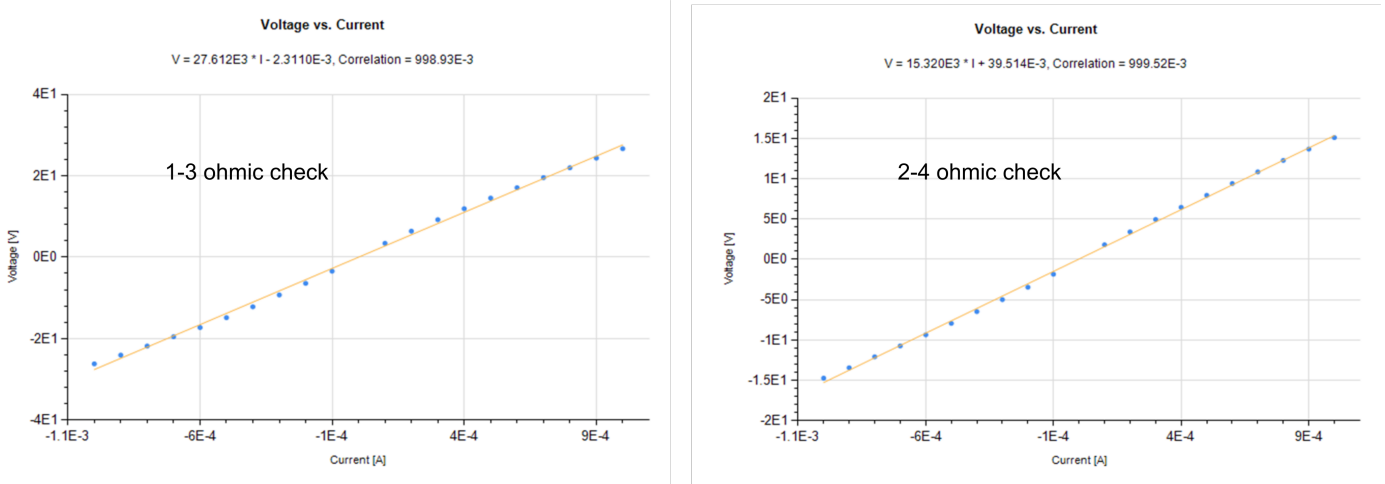

Fig. S21 Ohmic Check: Contacting $Zn_{1.2}Co_{1.8}O_{3.5}$ in the van der Pauw geometry shows ohmic linear behavior.

Lake Shore CRYOTRONICS

8400 Series

Resistivity measurement

Setup

Resistance measurement method:	High resistance
Excitation current	Manual
Current [mA]:	1
Current reversal:	Yes
General	
Sample geometry:	Geometry averaged
Average count:	10
Wait mode:	Auto
Measure current lead voltages:	No

Environment

	Start	Finish	Average	Status
Date	Monday, November 17,	Monday, November 17,		
Time	11:26:36 PM	11:28:36 PM		
Temperature [K]	300.2	300.2	300.2	Timeout
Field [T]	0.0000	0.0000		
Gate bias voltage [V]	0.0000E0	0.0000E0		
Gate bias current [A]	4.3397E-13	1.0931E-13		

Final average

		Geometry A		Geometry B	
		Mean value	**Limit**	**Mean value**	**Limit**
ρ	Resistivity [Ω·cm]	9.2146E-2		9.1875E-2	
ρ_{sheet}	Sheet resis/ vity [Ω/□]	4.3465E3		4.3337E3	
	F value	0.99		0.99	

Intermediate results

		Geometry A		Geometry B	
		R2134	**R3241**	**R4312**	**R1423**
	Resistance [Ω]	8.0865E2	1.1277E3	8.0570E2	1.1251E3
	Standard deviation of resistance [Ω]	1.1460E-2	1.6047E-2	9.8568E-3	1.9360E-2
	Voltage [V]	8.0859E-1	1.1276E0	8.0565E-1	1.1250E0
	Standard deviation of voltage [V]	5.2217E-6	6.5738E-6	4.2001E-6	1.3625E-5
	Current [A]	9.9992E-4	9.9991E-4	9.9993E-4	9.9994E-4
	Standard deviation of current [A]	1.2614E-8	1.2979E-8	1.1067E-8	1.2222E-8

Average measurements (I+)

		Geometry A		Geometry B	
		R2134	**R3241**	**R4312**	**R1423**
	Voltage [V]	8.0934E-1	1.1291E0	8.0427E-1	1.1264E0
	Standard deviation of voltage [V]	7.5468E-6	8.4175E-6	6.9433E-6	1.1666E-5
	Current [A]	1.0000E-3	1.0000E-3	1.0000E-3	1.0000E-3
	Standard deviation of current [A]	2.1591E-8	1.3743E-8	1.7665E-8	1.7115E-8
	Current lead voltage [DC V]	N/A	N/A	N/A	N/A

Average measurements (I-)

		Geometry A		Geometry B	
		R2134	**R3241**	**R4312**	**R1423**
	Voltage [V]	-8.0783E-1	-1.1261E0	-8.0703E-1	-1.1237E0
	Standard deviation of voltage [V]	7.2187E-6	1.0100E-5	4.7278E-6	2.4627E-5
	Current [A]	-9.9983E-4	-9.9982E-4	-9.9984E-4	-9.9985E-4
	Standard deviation of current [A]	1.3048E-8	2.2022E-8	1.3335E-8	1.7453E-8
	Current lead voltage [DC V]	N/A	N/A	N/A	N/A

Fig. S22 Resistivity at 300K: 8-fold probing in the van der Pauw geometry to obtain the isotropic resistivity of the 165 nm thick $Zn_{1.2}Co_{1.8}O_{3.5}$ on sapphire.

AC field Hall measurement

Setup

Resistance measurement method:	High resistance
Excitation field	
Frequency:	100mHz
Lock-in	
Response:	Slow
Sensitivity:	200µV
AC gain:	48dB
Excitation current	Manual
Current [µA]:	100
General	
Sample geometry:	Geometry averaged
Average count:	10
Wait mode:	Auto
Measure current lead and misalignment voltages:	No

Environment

	Start	Finish	Average	Status
Date	Monday, November 17,	Tuesday, November 18,		
Time	11:28:37 PM	12:31:51 AM		
Temperature [K]	300.2	300.2	300.2	Timeout
Field [T]	0.6251	0.6251		
Gate bias voltage [V]	0.0000E0	0.0000E0		
Gate bias current [A]	3.3276E-14	-8.1799E-14		

Final average

		Geometry C		Geometry D	
		Mean value	**Limit**	**Mean value**	**Limit**
V_H	Hall voltage [V]	1.2104E-6		1.3586E-6	
	Carrier type	P		P	
n	Carrier concentration [1/cm³]	1.5209E21		1.3550E21	
n_{sheet}	Sheet carrier concentration [1/cm²]	3.2243E16		2.8726E16	
R_H	Hall coefficient [cm³/C]	4.1039E-3		4.6062E-3	
R_{Hsheet}	Sheet Hall coefficient [cm²/C]	1.9358E2		2.1728E2	

Current reversal results

		Geometry C		Geometry D	
		P1-N1	**P2-N1**	**P1-N1**	**P2-N1**
V_H	Hall voltage [V]	1.2255E-6	1.1977E-6	1.2456E-6	1.4734E-6
	Phase [deg.]	-10.2	-15.3	-5.4	-1.3

Average measurements

		Geometry C			Geometry D		
		I+(P1)	**I-(N1)**	**I+(P2)**	**I+(P1)**	**I-(N1)**	**I+(P2)**
	Voltage [V]	1.7526E-5	1.8111E-5	1.7328E-5	1.1839E-5	1.2153E-5	1.2051E-5
	Standard deviation of voltage [V]	1.1100E-6	7.9734E-7	9.6260E-7	8.4987E-7	1.1740E-6	1.2841E-6
	Phase [deg.]	89.7	97.3	90.0	85.8	97.7	83.7
	Current [A]	1.0004E-4	-1.0001E-4	1.0004E-4	1.0004E-4	-1.0001E-4	1.0004E-4
	Misalignment voltage [DC V]	N/A	N/A	N/A	N/A	N/A	N/A
	Current lead voltage [DC V]	N/A	N/A	N/A	N/A	N/A	N/A

Fig. S23 AC-Hall measurement at 300K: the AC-Hall method developed by LakeShore (8400 HMS Series) allows to induce an AC-magnetic sinusoidal sweep of the magnetic field (amplitude maximum at 0.91 T, average at 0.6251 T, frequency 100 mHz), while the electric parameters (DC-current, voltage) are measured in DC-mode. Using this, the sensitivity is increased below $0.7 \cdot 10^{-6}$ V (high-sensitivity Hall voltage probing). Details of the measurements at 300K of the 165 nm thick $Zn_{1.2}Co_{1.8}O_{3.5}$ on sapphire are presented.

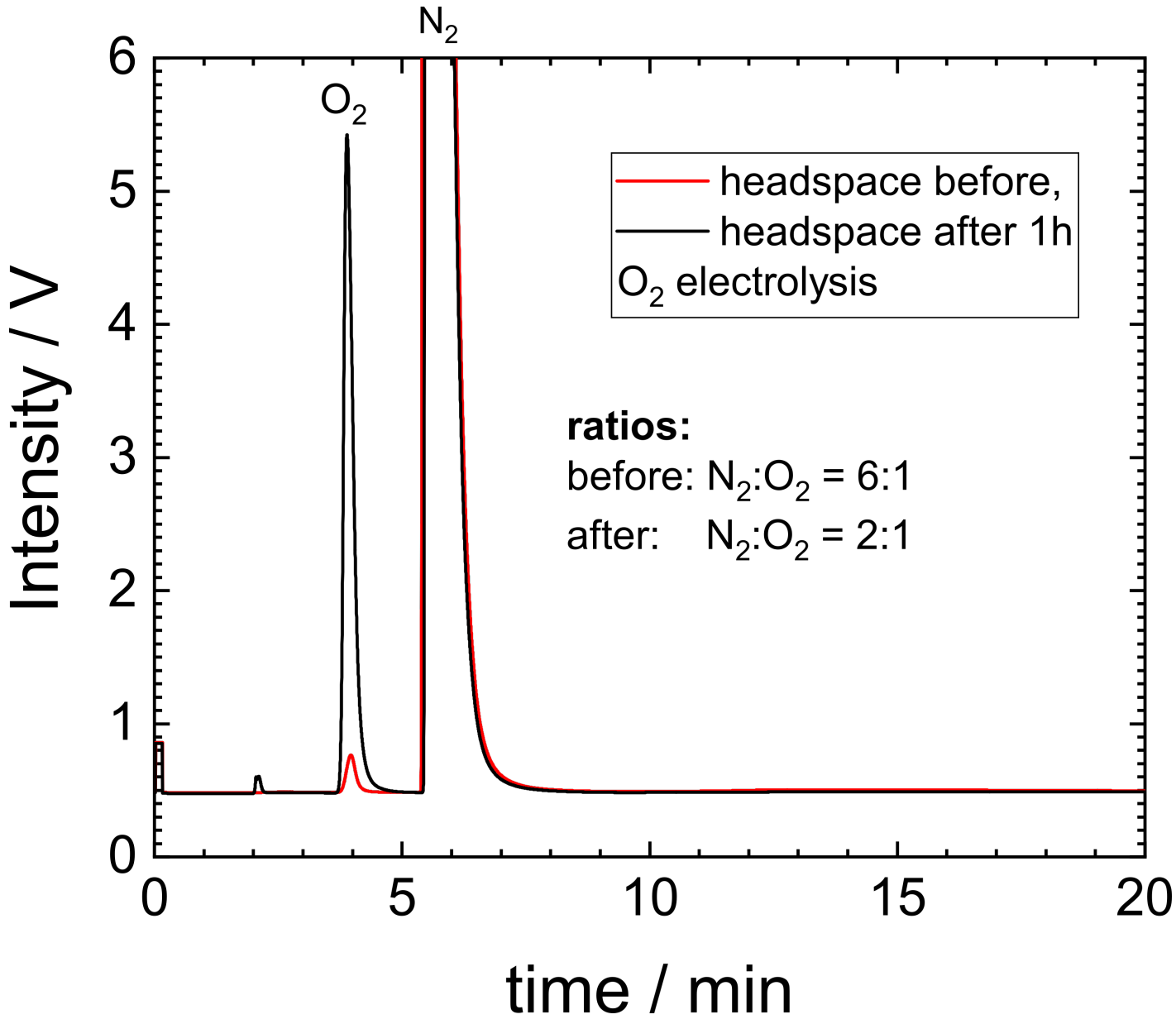

Fig. S24 Gas-chromatogram (He) of the anode headspace: Before and after composition of the headspace showing the rise of anodically produced O_2 gas.